Nanoscale

RSC Publishing

PAPER

View Article Online
View Journal | View Issue

A highly efficient microfluidic nano biochip based on nanostructured nickel oxide†

Cite this: *Nanoscale*, 2013, **5**, 2883

Md. Azahar Ali,[ab] Pratima R. Solanki,‡[a] Manoj K. Patel,[a] Hemant Dhayani,[a] Ved Varun Agrawal,*[a] Renu John*[b] and Bansi D. Malhotra*[c]

We present results of the studies relating to fabrication of a microfluidic biosensor chip based on nickel oxide nanorods (NRs-NiO) that is capable of directly measuring the concentration of total cholesterol in human blood through electrochemical detection. Using this chip we demonstrate, with high reliability and in a time efficient manner, the detection of cholesterol present in buffer solutions at clinically relevant concentrations. The microfluidic channel has been fabricated onto a nickel oxide nanorod-based electrode co-immobilized with cholesterol esterase (ChEt) and cholesterol oxidase (ChOx) that serves as the working electrode. Bare indium tin oxide served as the counter electrode. A Ag/AgCl wire introduced to the outlet of the microchannel acts as a reference electrode. The fabricated NiO nanorod-based electrode has been characterized using X-ray diffraction, Raman spectroscopy, HR-TEM, FT-IR, UV-visible spectroscopy and electrochemical techniques. The presented NRs-NiO based microfluidic sensor exhibits linearity in the range of 1.5–10.3 mM, a high sensitivity of 0.12 mA mM^{-1} cm^{-2} and a low value of 0.16 mM of the Michaelis–Menten constant (K_m).

Received 3rd November 2012
Accepted 16th January 2013

DOI: 10.1039/c3nr33459g

www.rsc.org/nanoscale

Introduction

Recent years have seen significant advances in the development of nanofluidic-based devices using one-dimensional (1D) nanostructured materials such as nanorods, nanotubes, nanowires and nanorings due to their novel properties.[1–3] These 1D nanostructures act as "electronic wires" that provide direct channels for the transport of electrons from an enzyme's active site to a current collector, and also improve enzyme loading due to the large-area scaffold. Among the 1D materials, rod-like geometries with well-defined crystal surfaces have been reported to be advantageous for the transport of charge carriers such as electrons and ions.[4–7]

The applications of microfluidic-based devices in biosensing have recently grown exponentially because of their exceptional merits over conventional devices in terms of portability, microscale bioanalysis, automated drug discovery, lower cost, quick diagnosis, and sample and reagent consumptions.[8,9] The integration of microfluidic devices (lab-on-a chip) with 1D nanorods provides a promising approach to the development of a smart biosensing chip that can be used to monitor desired analytes.[10,11] Many groups have reported the use of nanorods/nanotubes in biosensing, filtration and sample separation based on microfluidic devices.[12] Shi *et al.* have fabricated a low cost, high throughput and highly parallel mix-and-match nanodevice consisting of integrated nanopillar arrays using soft UV nanoimprint lithography and reactive-ion-etch techniques for application in long DNA molecule separation.[13] Koto *et al.* have developed molecular sensor arrays which consist of vertical germanium nanowires and function as field effect transistor (FET) based in a microfluidic channel on silicon, resulting in an improved sensing performance with a response time that is less than 10 s.[14]

Nanostructured nickel oxide (NiO) is an antiferromagnetic semiconductor with a wide band gap of ~3.6 eV that can be used in optoelectronic devices, FETs and biosensors.[15,16] NiO with different morphologies, including nanoparticles, nanostrips, nanorods, nanosheets and hollow spheres, have recently been used in various applications including biosensing.[16–20] Rod-like nanostructured NiO has been found to be stable in the environment and does not degrade with immobilization of biomolecules. The selective binding of molecules to nanostructured NiO and a Debye length which is comparable to the nanostructure may strongly influence its surface, giving rise to enhanced sensitivity.[21] In addition, NiO nanorods offer attractive properties such as a high isoelectric point (IEP; 10.8), high

[a]*Department of Science and Technology Centre on Biomolecular Electronics, Biomedical Instrumentation Section, National Physical Laboratory, Dr. K. S. Krishnan Marg, New Delhi-110012, India. E-mail: ved.varun@gmail.com*

[b]*Indian Institute of Technology Hyderabad, Ordnance Factory Estate, Yeddumailaram, Hyderabad, Andhra Pradesh 502205, India. E-mail: renujohn@iith.ac.in*

[c]*Department of Biotechnology, Delhi Technological University, Shahbad Daulatpur, Main Bawana Road, Delhi-42, India. E-mail: bansi.malhotra@gmail.com; Fax: +91 11 2781023; Tel: +91 11 7871043/1022 ext. 1609*

† Electronic supplementary information (ESI) available. See DOI: 10.1039/c3nr33459g

‡ Author's present address: Amity Institute of Nanotechnology, Amity University, Sector 125, Noida 201303, India

electro-catalytic activities and an increased sensitivity that enhances the intensity of an electrochemical signal.[22,23] Also, due to its improved electrical properties, the 1D NiO platform has a higher accumulation of charges on the surface compared with 2D nanostructured NiO.[18] A nanostructured NiO based genosensor for the diagnosis of *Visceral leishmaniasis* (kala-azar) has been developed and it has been found to be an excellent matrix for biomolecule immobilization.[24] Li *et al.* have used NiO hollow nanospheres for applications in glucose biosensing due to their highly specific active sites and electrocatalytic activity *via* the controlled precipitation of metal ions with urea using carbon microspheres as templates.[16]

Cholesterol is a part of the healthy dietary intake of fats and is a critical compound present in hormones, cell membranes, vitamin D and cell signalling. It is known that the ratio of total cholesterol to free cholesterol in a human blood sample is 70 : 30. A high cholesterol level in blood (more than 240 mg dL^{-1}) is linked to heart diseases that may be caused by blood vessel damage, nephrosis, diabetes mellitus, myxedema and jaundice. Researchers have shown that high cholesterol levels can affect macrophages, which are the part of the immune system that typically consumes pathogens and clears away dead cells. A low cholesterol level may result in hyperthyroidism, anaemia and maladsorption.[25–30] Other forms of cholesterol present in blood including very low density lipoproteins (VLDLs), intermediate density lipoproteins (IDLs), low density lipoproteins (LDLs) and triglycerides are clinically important as shown in a previous study.[27] The studies to date are largely focused on free cholesterol measurements. The development of state-of-the-art equipment for measuring total cholesterol has resulted in the commercialization of a "CardioChek" by Polymer Technology Systems Inc. which is based on a biochemical reaction that produces a color change when a blood sample is applied to a test strip. To the best of our knowledge, no efforts have been reported in the development of a microfluidic chip based low cost electrochemical device that can be used to monitor the amount of total cholesterol.

Cholesterol biosensors based on gold nanowires have been fabricated by electroplating an anodized alumina template integrated onto a microfluidic platform by a dielectrophoretic coating.[30] Singh *et al.* have demonstrated that chitosan modified NiO nanoparticles are good at accepting the electrons that are generated during the re-oxidation of cholesterol oxidase (ChOx) and are transferred to the electrode *via* the Ni^{2+}/Ni^{3+} redox couple. This results in an increased electrochemical current and the chitosan modified NiO nanoparticles exhibit a sensitivity of up to 0.808 μA mg^{-1} dL^{-1} cm^{-2}.[31] The nanostructured chitosan–NiO matrix shows a Michaelis–Menten constant (K_m) value of 0.67 mM which is attributed to the favorable conformation of ChOx and an increased loading onto the transducer surface. However, there is considerable scope to improve the total cholesterol biosensing performance in terms of the sensitivity, the K_m value, reducing the use of reagents/samples, reduced cost and decreased size of the device.

In this paper, we demonstrate a nickel oxide nanorods-based microfluidic nano biosensor chip that can be used to estimate total amount of cholesterol in a given test specimen. First, we describe the integration of the microfluidic biosensor chip for total cholesterol detection. We discuss the synthesis and characterization of NiO nanorods, followed by electrochemical characterization of the device. Finally, we summarize the merits and performance of the presented biosensor chip in estimating the amount of total cholesterol.

Results and discussions

Fabrication of the PDMS channels and electrodes, functionalization of the electrodes and integration of the compact device

Using wet chemical etching, microelectrodes are patterned onto desired ITO coated glass plates. Nickel oxide nanorods (NRs-NiO) are synthesized using the standard co-precipitation technique and deposited onto the microelectrode by a dip coating technique. The nickel oxide nanorods-based electrode is co-immobilized with cholesterol esterase (ChEt) and cholesterol oxidase (ChOx) and it serves as the working electrode (ChEt–ChOx/NR-NiO/ITO). The bare ITO microelectrode served as the counter electrode. Polydimethylsiloxane (PDMS) channels of dimensions 200 μm × 200 μm × 2 cm (width × height × length) have been fabricated using standard photolithography technique and tightly sealed onto the glass substrate containing ITO and the ChEt–ChOx/NR-NiO/ITO electrode (Scheme 1) that acts as the microfluidic biosensor chip. The two electrodes and microchannels are embedded in the same chip. The inlet reservoir of the microchannel is used to introduce the syringe pump to maintain a constant flow rate of 10 μL min^{-1}. A Ag/AgCl wire is introduced into the outlet reservoir of the microchannel acted as a reference electrode. More details on the fabrication are explained in the materials and methods section.

Structural characterization of NiO nanorods

X-ray diffraction (XRD) studies [Fig. 1(i)] reveal the purity and crystallinity of the synthesized nickel oxide nanorods (NRs-NiO) with a face-centred cubic system (a of 4.1 Å) and space group *Fm3m* (225), [JCPDS Card no. 78-0423]. All the peaks are assigned to the diffraction pattern resulting from the (111), (200), (220) and (222) planes of the cubic NiO. This observation indicates that the resultant NiO nanorods are mainly dominated by (111) facets. The intensity ratio between the (111) and (200) planes of the NRs-NiO [inset: Fig. 1(i)] is calculated to be 5.2, which is much higher than that of bulk NiO (1.45), indicating preferred crystallization along the (111) plane. The d_{111} value of the NiO nanorods, which is found to be 0.241 nm for the (111) plane, is the same as that shown in the HR-TEM studies. The peaks seen at 50.9° and 60.5° corresponding to the (124) and (143) planes are due to the ITO coating on the glass substrate.

The Raman spectrum of the NR-NiO powder shows several bands above 400 cm^{-1} at room temperature (25 °C) [Fig. 1(ii)]. The vibrational band due to one phonon (1P) at 507 cm^{-1} corresponds to the transverse optical (TO) mode arising due to the excitation wavelength of 532 nm. This 1P band has a very

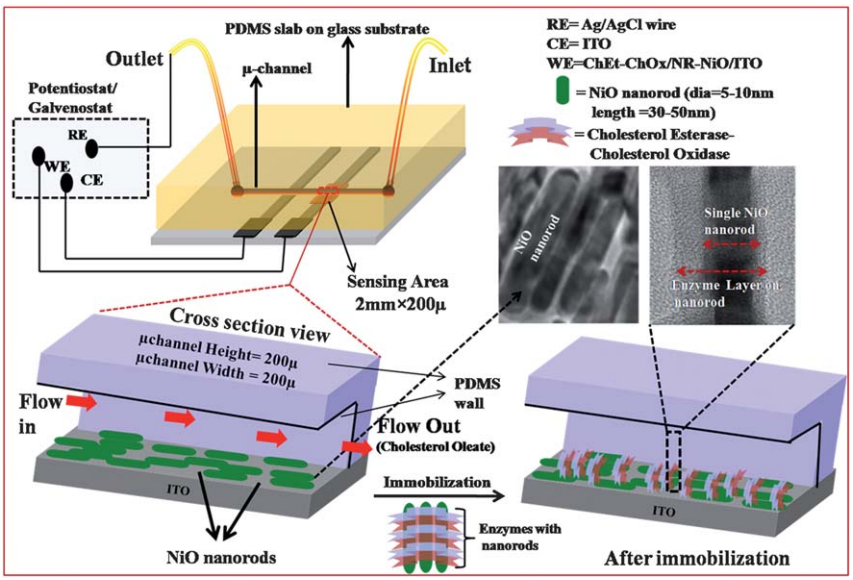

Scheme 1 The microfluidic chip used for the detection of total cholesterol (the ordered arrangement of this chip is just an assumption to aid the clarity of the figure).

small intensity indicating good crystallinity. The peaks due to two phonon (2P) seen at ~713 cm^{-1} and ~1090 cm^{-1} are assigned to 2TO modes and 2LO (longitudinal optical) modes, respectively. The band found at ~713 cm^{-1} exhibits a low intensity at room temperature indicating the presence of the NRs-NiO.[32] In the ultra violet (UV)-visible spectrum a strong peak is observed at ~379 nm which corresponds to the intra-3d transition of Ni^{2+} in the NiO structure [inset: Fig. 1(ii)] as compared to that of the bulk NiO (484 nm).[24] This result shows a blue shift to 105 nm indicating the formation of the nanostructured NiO. This is due to the fact that the nanostructures are laterally quantum confined and occupy energy levels that are different from the traditional continuum of energy levels or bands found in a bulk material.

In the Fourier transform-infrared (FT-IR) studies [Fig. 2], the infrared peak found at 545 cm^{-1} in the finger print region (curve a) corresponds to the Ni–O bending vibration. The dominant peak found at 1263 cm^{-1} arises due to bicarbonate (HCO_3) stretching on the NR-NiO film. The absorption bands seen at ~1000 to 2500 cm^{-1} are assigned to the O–C═O symmetric and asymmetric stretching vibrations and the C–O stretching vibration, which indicates that the NiO nanorods tend to strongly physically adsorb CO_2. The presence of a peak at 1632 cm^{-1} [curve (b)] corresponds to the amide 1 band of ChEt and ChOx indicating that emzymes have immobilized onto the film. The band found at 545 cm^{-1} for NiO is shifted to 600 cm^{-1} due to incorporation of the enzyme (ChEt and ChOx) molecules. The band found at (3500–3700 cm^{-1}) is assigned to the O–H stretching vibration in the NiO film.

Morphological characterization of the NiO nanorods and their functionalization

High resolution-transmission electron microscopy (HR-TEM) studies have been conducted to unravel the NiO microstructural shape, size and surface morphology. For the HR-TEM studies,

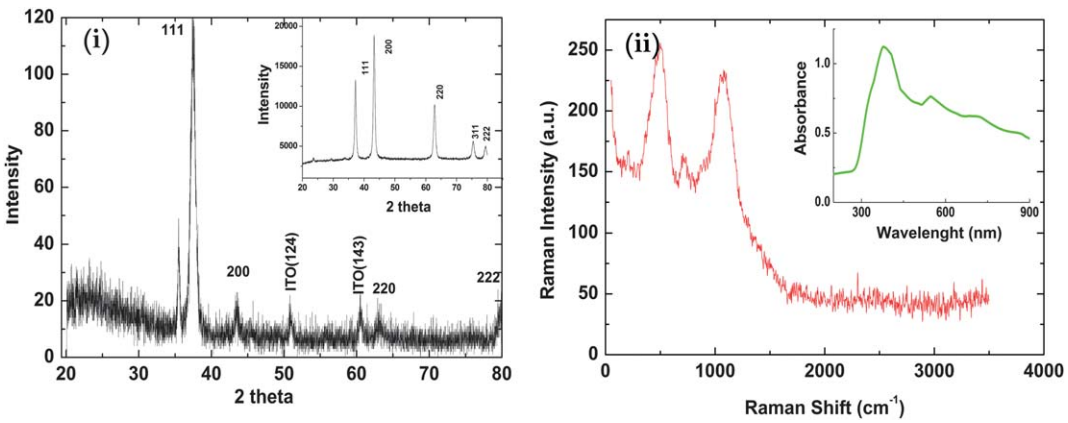

Fig. 1 (i) The X-ray diffraction pattern of the NRs-NiO on the ITO film (inset: the powder XRD pattern of the NiO nanorods) and (ii) Raman spectroscopy studies of the NiO nanorods (inset: UV-visible spectroscopy studies of the NRs-NiO/ITO film).

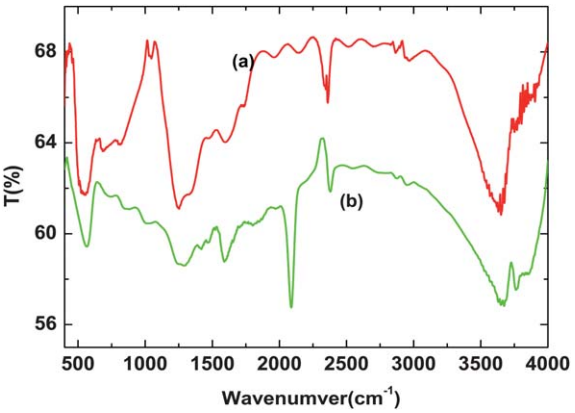

Fig. 2 FTIR spectra of (a) the NR-NiO/ITO film and (b) the ChEt–ChOx/NR-NiO/ITO film.

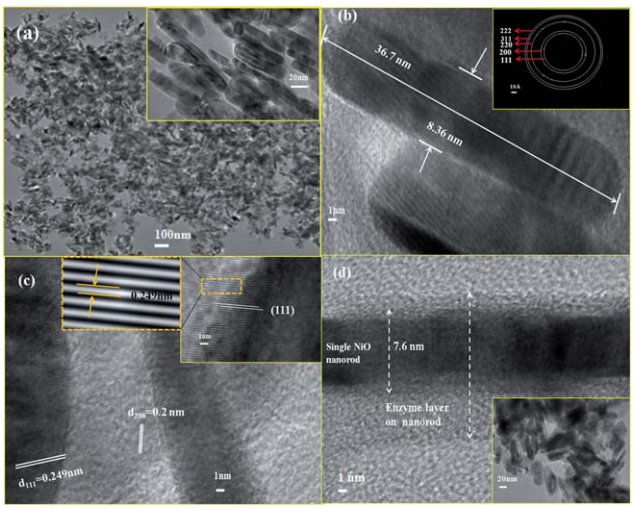

Fig. 3 HR-TEM analysis of (a) the synthesized NiO nanorods (inset: a zoomed image of the nanorods), (b) the single nanorods micrograph with length 36.7 nm and width 8.3 nm (inset: SAED pattern of the NiO nanorods), (c) lattice fringes of the as-synthesed NRs-NiO with different planes (inset: lattice fringe for the (111) plane and the zoomed image) and (d) ChEt–ChOx immobilization onto NRs-NiO (inset: image at low resolution).

NiO nanorods dispersed in methanol are deposited onto the carbon coated copper grid by drop casting and are dried in an open atmosphere. Fig. 3(a) shows agglomeration of the NiO nanorods. The majority of the NiO nanorods exhibit a nearly straight appearance [inset: Fig. 3(a)]. The solid rods-like structures tend to organise the long axes parallel to each other. The structural orientation of the individual nanorod (length = ~38 nm; diameter = ~8 nm) has been investigated *via* high resolution TEM [Fig. 3(b)] which shows presence of the moire fringes. These results reveal the presence of nanorods with conical tips in NiO. These NiO nanorods exhibit a low aspect ratio (length-to-width ratio) of ~4 indicating an elongated nanostructure. The clear lattice fringes illustrate that the nanorods are highly crystalline in nature [Fig. 3(c)]. The spacing between the two adjacent fringes for different planes is found to be 0.245 nm and 0.20 nm [Fig. 3(c)]. The interplanar spacing of 0.245 nm [inset: Fig. 3(c)] corresponds to the (111) plane revealing anisotropic growth of the nanorods along the (111) direction. The selected area electron diffraction (SAED) pattern consists of five diffraction rings with different radii [inset: Fig. 3(b)]. The diameter of the diffraction rings in the SAED pattern is proportional to $\sqrt{h^2 + k^2 + l^2}$. The 1st, 2nd, 3rd, 4th and 5th rings correspond to the (111), (200), (220), (311) and (222) planes, respectively. These solid rod-like shapes of NiO may be beneficial for enzyme loading due to the increased surface area. A thick transparent layer of visible enzymes (ChOx and ChEt) containing a consistent distribution of ChOx–ChEt is clearly seen on the individual nanorods [Fig. 3(d)]. These results indicate that the NiO nanorods act as a substrate for biomolecules.

Electrochemical characterization

The electrochemical impedance spectroscopy (EIS) technique has been used to measure the impedance of the electrode–electrolyte interface in response to a small AC signal as a function of frequency (0.01 to 10^5 Hz) [Fig. 4(i)]. The modification of an electrode surface results in a change in the value of the charge transfer resistance (R_{CT}). The diameter of a semicircle plot in an EIS spectra gives a value of R_{CT} that reveals the electron transfer kinetics of the redox probe at the electrode/electrolyte interface. The Nyquist diagrams of the EIS curve show that the R_{CT} value of the NR-NiO/ITO electrode is 19 kΩ (curve a) compared to that of the ChEt–ChOx/NR-NiO bioelectrode (curve b). This is due to the presence of the NiO nanorods on the electrode surface that are insulating in nature and therefore impede/sterically hinder diffusion of the ferri/ferro cyanide ($Fe^{2+/3+}$) ions from bulk solution to the electrode surface, resulting in enhanced charge transfer resistance. After the co-immobilization of ChEt and ChOx onto the NR-NiO electrode surface, the charge transfer resistance (R_{CT}) decreases to 8.08 kΩ (curve b) implying that the enzyme molecules are indeed absorbed onto the NR-NiO/ITO surface and are strongly immobilized on to the NiO nanorods present on the electrode surface. This low value of R_{CT} (curve b) is due to the fact that the NiO nanorods provides enhanced catalytic activity of the enzyme and induce favourable electron transfer kinetics in the NiO nanorods that enable a rapid oxidation/reduction of the $[Fe(CN)_6]^{3-/4-}$ ions that reach the electrode surface. In addition, the NiO nanorods also establish electronic pathway that reduces the tunnelling distance for the diffuse ions (or electrons) between the enzyme's active site and the electrode. This reveals that the bioelectrode is more conductive in nature, which is in agreement with results of the cyclic voltammetry studies.

Cyclic voltammetry (CV) studies are carried out on the NR-NiO/ITO electrode and the ChEt–ChOx/NR-NiO/ITO bioelectrode in the potential range from −0.8 V to +0.9 V in PBS buffer containing 5 mM $[Fe(CN)_6]^{3-/4-}$ at a scan rate of 30 mV s^{-1} [Fig. 4(ii)]. In the cyclic voltammogram, the ChEt–ChOx/NR-NiO/ITO bioelectrode shows well-defined oxidation and reduction peaks at +0.399 V and −0.14 V, respectively, with a

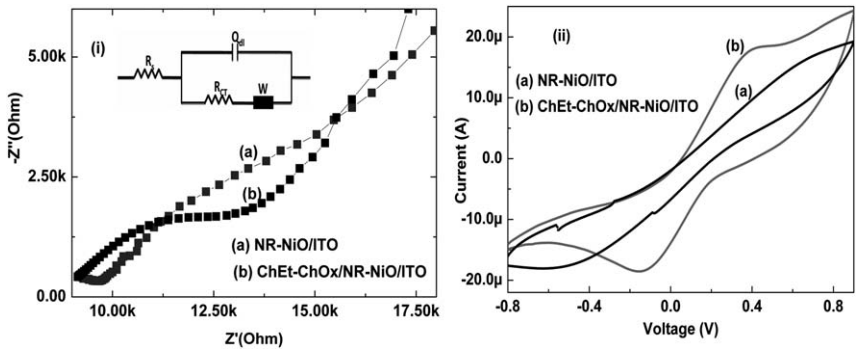

Fig. 4 (i) Electrochemical impedance spectroscopy of (a) the NR-NiO/ITO electrode and the ChEt–ChOx/NR-NiO/ITO bioelectrode (inset: Randles equivalent circuit model for EIS measurement, where R_s = solution resistance, R_{CT} = charge transfer resistance, Q_{dl} = constant phase element or double layer capacitance, W = Warburg impedance). (ii) The cyclic voltammogram of (a) the NR-NiO/ITO electrode and (b) the ChEt–ChOx/NR-NiO/ITO bioelectrode in PBS solution (50 mM, pH 7.0, 0.9% NaCl) containing 5 mM $[Fe(CN)_6]^{3-/4-}$.

peak-to-peak separation of 0.53 V. These anodic/cathodic peaks arise due to the presence of the nanorods that provide confined 1D channels for the transportation of electrons from the enzyme's active site to the electrode. The anodic peak current of the ChEt–ChOx/NR-NiO/ITO bioelectrode is higher (curve b) as compared to that of the NR-NiO/ITO electrode (curve a) which indicates a fast electron communication between the matrix and the ChEt and ChOx molecules. This indicates that nanorods with a larger surface area facilitate a higher mass diffusion efficiency due to the electrochemical activation of the enzyme's active site resulting in enhanced redox current. The high electrocatalytic activity of the NiO nanorods could improve the performance of the cholesterol biosensor.

CV studies of the ChEt–ChOx/NR-NiO/ITO bioelectrode have been carried out as a function of scan rate (30–110 mV s^{-1}) (Fig. 5). The magnitude of current of both the anodic peak (I_{pa}) and the cathodic peak (I_{pc}) observed for the ChEt–ChOx/NR-NiO/ITO bioelectrode increases linearly with scan rate (inset: Fig. 5) indicating quasi-reversible diffusion controlled behavior. It can be seen that the anodic potential shifts towards the positive side and the cathodic peak potential (inset: Fig. 5) shifts in the reverse direction. The values of the slope, intercept and correlation coefficient are given by eqn (1) and (2).

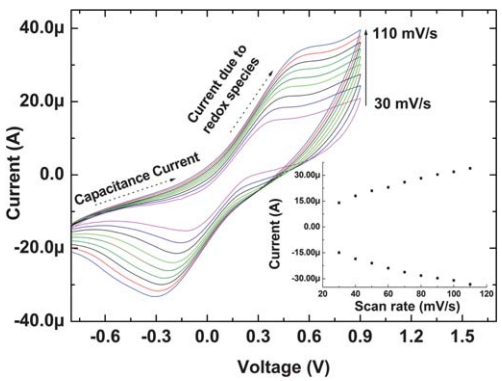

Fig. 5 The cyclic voltammogram of the ChEt–ChOx/NR-NiO/ITO bioelectrode as a function of scan rate [30–110 mV s^{-1}] in ascending order in PBS solution containing 5 mM $[Fe(CN)_6]^{3-/4-}$.

$$I_{pa(ChEt–ChOx/NR\text{-}NiO/ITO)} = 8.14\ \mu A + 0.243\ \mu A\ mV^{-1}\ s \times \text{scan rate (mV } s^{-1}); r^2 = 0.9993 \quad (1)$$

$$I_{pc(ChEt–ChOx/NR\text{-}NiO/ITO)} = -9.6\ \mu A - 0.22\ \mu A\ mV^{-1}\ s \times \text{scan rate (mV } s^{-1}); r^2 = 0.990 \quad (2)$$

The surface concentration (C_0^*) of the ChEt–ChOx/NR-NiO/ITO bioelectrode has been estimated using eqn (3),

$$i_p = 0.227nFAC_0^*k^0\exp\left[\frac{\alpha n_a F}{RT}\left(E_p - E_0^{'}\right)\right] \quad (3)$$

where i_p is the anodic peak current, n is the number of electrons transferred [eqn. (1)], F is the Faraday constant (96485.34 C mol^{-1}), R is the gas constant (8.314 J mol^{-1} K^{-1}), A is the area of electrode surface (cm^2), C_0^* is the surface concentration of the ionic species in the film (mol cm^{-2}), E_p is the peak potential and $E_0^{'}$ is the formal potential. $\alpha n_a F/RT$ and k^0 (rate constant) correspond to the slope and intercept of the $\ln(i_p)$ *versus* $(E_p - E_0^{'})$ curve at different scan rates. The values of surface concentration for the ChEt–ChOx/NR-NiO/ITO bioelectrode have been found to be 5.6×10^{-7} mol cm^{-2}.

Effect of flow rate

Fig. 6 shows the plot of diffusivity of the $(Fe^{2+/3+})$ ions in the NR-NiO/ITO electrode and flow rate [10–70 μL min^{-1}] using CV in PBS (50 mM, pH 7.0, 0.9% NaCl) containing $[Fe(CN)_6]^{3-/4-}$ at a scan rate of 30 mV s^{-1}. It has been found that the flow rate influences the charge carriers (electrons) diffusion towards the electrode. The anodic current is found to increase with the increasing flow rate of the PBS buffer controlled by application of a positive pressure (syringe pump) [inset: Fig. 6]. The diffusion coefficient (or diffusivity) of the electrolyte ions for each CV response at different flow rates has been estimated using the Randles–Sevcik equation [eqn (4)],

$$i_p = (269\ 000)n^{3/2}AD^{1/2}Cv^{1/2} \quad (4)$$

where i_p = redox peak current (A), n = number of electrons transferred in the redox event [n=1, in this case], A = electrode

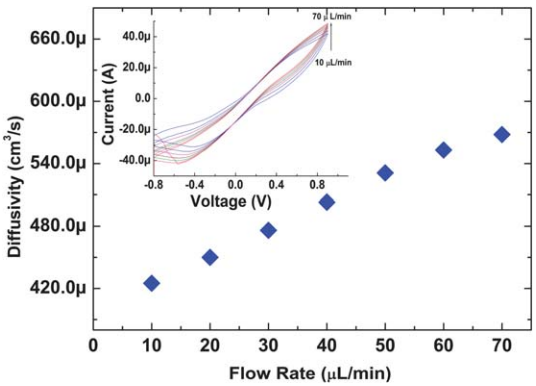

Fig. 6 The diffusivity of the NR-NiO/ITO electrode at different flow rates using a syringe pump [inset: the CV response of the NR-NiO/ITO electrode at different flow rates (10–70 μL min^{-1})].

area (cm^2), D = diffusion coefficient (cm^2 s^{-1}), C = concentration of redox species (mol cm^{-3}) and ν = scan rate (mV s^{-1}). It has been observed that diffusivity of the redox species increases at higher buffer flow rates due to improved mass transport resulting from the increased fluid velocity.[33] However, Collier and Hart have demonstrated that the response time decreases with the increasing flow rate of the buffer solution and have shown that the response time is inversely proportional to the flow rate.[34] Thus, we have carried out all the electrochemical studies at an optimized flow rate of 10 μL min^{-1}.

Electrochemical response studies

The cyclic voltammetry response of the ChEt–ChOx/NR-NiO/ITO bioelectrode has been conducted with successive addition of cholesterol oleate at the inlet of the microchannel at a scan rate of 30 mV s^{-1} and under optimum flow rate conditions (10 μL min^{-1}) (inset: Fig. 7). It has been observed that the anodic peak current increases when the concentration of cholesterol oleate (cholesterol esters) increases from 25 to 400 mg dL^{-1} (Fig. 7). In

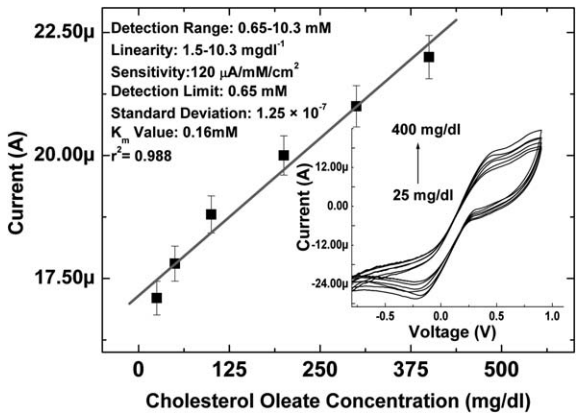

Fig. 7 The microfluidic sensor linear fit curve between the peak current response of CV and different concentration of cholesterol oleate in the range 25–400 mg dL^{-1} attached to the inlet of the microfluidic chip (inset: the CV response of the ChEt–ChOx/NR-NiO/ITO bioelectrode as a function of cholesterol oleate concentration introduced using a syringe pump at a flow rate of 10 μL min^{-1}).

the proposed biochemical reaction, cholesterol esters (cholesterol oleate) are hydrolyzed *via* cholesterol esterase (ChEt) into cholesterol (or 3β-hydroxysteroids) and fatty acid. Again utilizing flavin adenine dinucleotide (FAD), ChOx catalyses the oxidation and isomerization of 3β-hydroxysteroids containing a *trans* double bond Δ^5–Δ^6 in the steroid ring to give the corresponding Δ^4-3-ketosteroid and hydrogen peroxide (H_2O_2).[35] H_2O_2 produces electrons *via* its re-oxidation at 0.45 V. Thus during cholesterol detection, the NiO nanorods directly accept electrons from the reduced ChOx molecules in the presence of $[Fe(CN)_6]^{3-/4-}$ as the mediator (Scheme S1, ESI†). This integrated microfluidic sensor exhibits detection in the range of 0.65 mM to 10.3 mM with an excellent sensitivity of 120 μA mg^{-1} dL^{-1} cm^{-2} compared to that of other microfluidic devices as shown in Table 1. The detection limit is found to be 0.65 mM and the value of the enzyme–substrate kinetics parameter (Michaelis–Menten constant, K_m) has been estimated using the Lineweaver–Burke plot [Fig. S1, ESI†] revealing the affinity of the enzyme for the desired analyte. From Table 1, it can be seen that the detection range of NiO nanorods based cholesterol sensor (0.64–10.3 mM) is better than that of carbon nanotubes and gold nanowires based microfluidic devices, (1.28–10 mM and 1.293–6.4 mM, respectively).[38,39] The Lineweaver–Burke equation [eqn (5)] is given as

$$\frac{I}{I_{ss}} = \frac{1}{I_{max}} + \frac{K_m}{I_{max} C} \quad (5)$$

where I_{ss} is the steady-state current after the addition of the substrate, C is the bulk concentration of the substrate, and I_{max} is the maximum current measured under saturated substrate conditions. It may be noted that K_m is dependent on both the matrix and the method of immobilization of enzymes that in turn may bring about conformational changes resulting in different values of K_m. Besides this, the value of K_m for the bound enzyme can be lower or higher than that of the purified enzyme. We have obtained a value of K_m for the ChEt–ChOx/NR-NiO/ITO bioelectrode of 0.16 mM, which is smaller than the reported value. The lower K_m value indicates a high affinity for cholesterol to associate with ChOx and ChEt on the NR-NiO/ITO surface for faster biochemical reaction. This microfluidic sensor achieves 95% of the steady-state current in less than 5 s indicating a fast electron exchange between the ChEt–ChOx and the NR-NiO/ITO electrode.

The effect of potential interferents such as ascorbic acid (AA), uric acid (UA), glucose (G), lactic acid (LA) and urea present in blood samples at normal concentrations on the response of the ChEt–ChOx/NR-NiO/ITO bioelectrode has been investigated using CV at the same flow rate (Fig. S2, ESI†). The change in the oxidation current has been measured in PBS containing an equal amount (1 : 1) of cholesterol oleate (200 mg dL^{-1}) and interferent using eqn (6),[36]

$$\%\text{Inter} = I_{chol} - I_{int}/I_{chol} \quad (6)$$

where I_{chol} and I_{int} are the changes in the current corresponding to the cholesterol oleate and the mixture of cholesterol oleate with the desired intereferent. As illustrated (Fig. S2, ESI†), the

Table 1 The sensing characteristics of the cholesterol biosensor along with those reported in the literature

Working electrode	Microfluidics used	Detection range (mM)	Lower detection limit (mM)	Sensitivity	K_m value (mM)	Reference
CNT	Yes	1.25–10.0	0.25	0.0512 nA mM^{-1}	—	38
Au wire	Yes	1.293–6.4	0.1	—	—	39
Gold nanoparticles	No	Up to 2.1	0.060	0.13 μA mM^{-1}	2.94	40
ZnO	No	Up to 7.7	0.012	1.53 nA mM^{-1}	0.22	41
Aligned Au nanowires	Yes	0.01–0.060	—	0.85 μA mM^{-1}	17.1	42
Anatase–TiO_2	Yes	0.64–10.3	1.2	94.65 μA mM^{-1}	0.14	43
NiO nanorods	Yes	0.64–10.3	0.65	120 μA mM^{-1}	0.16	Present work

effects are negligible except in the case of uric acid. The storage stability of the ChEt–ChOx/NR-NiO/ITO bioelectrode has been determined by measuring the change in the current response at a regular interval of 1 week for about 2 months (Fig. S3, ESI†). The ChEt–ChOx/NR-NiO/ITO bioelectrode is stored at 4 °C when not in use. It has been found that the bioelectrode exhibits a 95% response after about 3 weeks.

Conclusions

A microfluidic-based nano biosensor chip using nickel oxide nanorods functionalized with ChEt and ChOx has been fabricated for the detection of the amount of total cholesterol in a sample. These NiO nanorods have been successfully integrated with the microenvironment module for precise and accurate detection of the bioanalyte that can be used to perform bioanalyte analysis. The laminar flow regime influences the diffusivity towards the electrode *via* nanorods and the enzyme's active site due to a low Reynold number (0.82) at a flow rate of 10 μL min^{-1} through the microchannel. NiO nanorods integrated with the miniaturized microfluidic device offer an improved sensitivity for total cholesterol detection. Studies show that there is no significant change in the redox current of this microfluidic sensor on introducing interferents along with the analyte. We have achieved the production of a miniaturized and low cost sensor with improved biosensing properties using the proposed microfluidic chip. Efforts are under way to explore the use of this nanorods-based microfluidic chip for the detection of other multianalytes simultaneously, including low density lipoproteins (LDLs), very low density lipoprotein (VLDLs) and triglyceride *etc.*

Experimental details

Materials and methods

Cholesterol oleate solution (400 mg dL^{-1}) is first dissolved in 1% polidocanol (Brij) as a surfactant with heating/stirring resulting in a clear and colourless suspension and the final volume is made by the addition of 0.9% NaCl solution. Furthermore, different concentrations of cholesterol oleate varying from 25 to 400 mg dL^{-1} have been prepared in a 0.9% NaCl solution. Cholesterol oxidase (ChOx), cholesterol esterase (ChEt), cholesterol oleate, nickel nitrate $[Ni(NO_3)_2]\cdot H_2O$ and potassium hydroxide (KOH) have been purchased from Sigma Aldrich, USA. The SU8-100 negative photoresist and the SU-8 developer are purchased from Microchem (Newton, MA, USA).

Synthesis of NiO nanorods

0.5 M $[Ni(NO_3)_2]\cdot 6H_2O$ (nickel nitrate) is dissolved in deionized water and 0.2 M KOH (potassium hydroxide) solution is added drop wise with constant stirring. Nickel hydroxide $[Ni(OH)_2]$ forms as a green precipitate at pH ~11.8. Furthermore, it is washed until pH 7.0 is achieved. Excess solvent is evaporated and the precipitate is dried at 80 °C for about 24 h resulting in formation of a transparent viscous solution of nickel hydroxide. The transparent thick gel-like $Ni(OH)_2$ solution is deposited onto the patterned ITO on the glass substrate *via* dip coating.

PDMS microchannel fabrication

The PDMS microchannels were fabricated by a soft lithography technique. The negative SU-8 photoresist is spin coated (~200 μm thick) onto a silicon wafer using the photoresist spinner. The wafer is then heated at 100 °C for evaporation of the solvent that is used to expose UV radiation through a desired mask. It is again heated (110 °C) to selectively cross-link in the exposed region of the SU-8. The unexposed SU-8 is removed *via* a SU-8 developer that forms the master. Prior to being used, the wafer is cleaned in acetone and is subsequently exposed to fuming HNO_3. The PDMS prepolymer and the curing agent (Sylgard 184, Dow Corning) are mixed in a 10 : 1 ratio (v/v), degassed under vacuum, poured onto the master, and cured at 80 °C for about 30 min. The PDMS replica is then carefully peeled off the master. The channel height and width are 200 μm each and the length is 2 cm. The reservoirs are fabricated by punching holes at desired positions in the PDMS slab.

ITO microelectrode fabrication

The ITO coated glass substrate (thickness ~150 to 300 Å) with a resistance of 70–100 Ω has been used to fabricate the desired microelectrode *via* wet chemical etching.[37] To obtain the desired two patterned electrode, the indium tin oxide (ITO) glass substrate is first selectively masked using a transparent masking tape (commercially available cellotape). The masked ITO/glass substrate is dipped in the etchant [HNO_3 : HCl : H_2O (1 : 10 : 10)] solution for about 15 minutes. The ITO layer is then removed from the glass substrate (mask free ITO layer only). The obtained ITO pattern on the glass substrate is then cleaned

with acetone and sonicated with acetone (10 min), which is followed by washing with dichloromethane (10 min), and finally with water (2 min) several times.

This glass substrate containing the desired electrodes (0.6 × 0.2 cm^2) is hydrolyzed using a mixture of $H_2O : H_2O_2 : NH_3$ (5 : 1 : 1), washed with deionized water and dried in an oven at 100 °C for about 4 h. The entire glass substrate is again masked. The masking tape is selectively removed from one patterned ITO electrode. This substrate is dipped into the transparent, thick $Ni(OH)_2$ solution and dried at 110 °C for about 1 hour after which the remaining cellotape film is removed from the substrate. Finally, the glass substrate containing $Ni(OH)_2$/ITO and bare ITO electrodes are annealed at 400 °C under ambient conditions for about 2 h to remove any solvent. This results in the formation of nickel oxide nanorods on patterned ITO.

Enzyme co-immobilization

1 mg mL^{-1} cholesterol esterase (ChEt) and 1 mg mL^{-1} cholesterol oxidase (ChOx) are mixed in a 1 : 1 ratio. 10 μL solution of this mixture is uniformly spread onto the NR-NiO/ITO microelectrode *via* physical adsorption (Scheme 1) and kept in a humid environment for 12 h at 4 °C. The values of the ionization electron potential (IEP) of the NiO and the enzyme (ChEt–ChOx) are found to be 10.8 and 5.3, respectively. Electrostatic interactions occur as the NiO matrix is positively charged and the enzyme is negatively charged. The ChEt–ChOx/NR-NiO/ITO bioelectrode is washed with 50 mM PBS (pH 7.0) to remove any unbound enzyme from the electrode surface. The bioelectrode is stored at 4 °C when not in use.

Instrumentation

The characterization of the NiO nanorods and the ChEt–ChOx/NR-NiO/ITO bioelectrode was carried out using X-ray diffraction (XRD, Cu Kα radiation, Rigaku), Raman spectroscopy and high resolution-transmission electron microscopy (HR-TEM, JEOL JEM-2000 EX). Fourier-transform infrared spectroscopic measurements (FT-IR) (Perkin-Elmer, Model 2000) have been carried out for the characterization of the NR-NiO/ITO electrode and the ChEt–ChOx/NR-NiO/ITO bioelectrode. The electrochemical studies have been performed using an Electrochemical Analyzer (AUT-84275) in phosphate buffer saline (PBS, pH 7.0) containing 5 mM $[Fe(CN)_6]^{3-/4-}$ as a redox probe.

Acknowledgements

We thank Director NPL, New Delhi, India for the facilities. Md Azahar Ali, M. K. Patel and Hemant Dhyani are thankful to CSIR, India, for the award of a Senior Reaserch Fellowship. The authors are also thankful to the Advance Instrumentation and Research Facilities (AIRF), JNU, New Delhi for TEM analysis. V. V. Agrawal is thankful to CSIR Empower project for funding. The authors are thankful to Ranjith Ramadurai, IIT Hyderabad for Raman studies. The financial support received from the Department of Science & Technology (Grant No. DST/TSG/2008/18) and Indian Council of Medical Research (Grant No. 513/8/91/GM/2010-RHN).

References

1 H.-M. Kim, T. W. Kang and K. S. Chung, *Adv. Mater.*, 2003, **15**, 567.
2 Y. Huang, X. Duan, Y. Cui, L. J. Lauhon, K.-H. Kim and C. M. Lieber, *Science*, 2001, **294**, 1313.
3 J. C. Johnson, H.-J. Choi, K. P. Knutsen, R. D. Schaller, P. Yang and R. J. Saykally, *Nat. Mater.*, 2002, **1**, 106.
4 M. D. Scanlon, U. Salaj-Kosla, S. Belochapkine, D. MacAodha, D. Leech, Y. Ding and E. Magner, *Langmuir*, 2012, **28**, 2251.
5 R. S. Devan, R. A. Patil, J.-H. Lin and Y.-R. Ma, *Adv. Funct. Mater.*, 2012, **22**, 3326.
6 A. Cattani-Scholz, D. Pedone, M. Dubey, S. Neppl, B. Nickel, P. Feulner, J. Schwartz, G. Abstreiter and M. Tornow, *ACS Nano*, 2008, **2**, 1653.
7 R. Wang, C. Ruan, D. Kanayeva and K. Lassiter, *Nano Lett.*, 2008, **8**, 2625.
8 S. Srivastava, P. R. Solanki, A. Kaushik, M. A. Ali, A. Srivastava and B. D. Malhotra, *Nanoscale*, 2011, **3**, 2971.
9 V. N. Goral, N. V. Zaytseva and A. J. Baeumner, *Lab Chip*, 2006, **6**, 414.
10 X.-J. Huang and Y.-K. Choi, *Sens. Actuators, B*, 2007, **122**, 659.
11 J. Kim, Z. Li and I. Park, *Lab Chip*, 2011, **11**, 1946.
12 J. Chen, J. Lib and Y. Sun, *Lab Chip*, 2012, **12**, 1753.
13 J. Shi, A. P. Fang, L. Malaquin, A. Pépin, D. Decanini, J. L. Viovy and Y. Chen, *Appl. Phys. Lett.*, 2007, **91**, 153114.
14 M. Koto, P. W. Leu and P. C. McIntyre, *J. Electrochem. Soc.*, 2009, **156**, K11.
15 G. Malandrino, L. M. S. Perdicaro, I. L. Fragal, R. L. Nigro, M. Losurdo and G. Bruno, *J. Phys. Chem. C*, 2007, **111**, 3211.
16 C. Li, Y. Liu, L. Li, Z. Du, S. Xu, M. Zhang, X. Yin and T. Wang, *Talanta*, 2008, **77**(1), 455.
17 H. Pang, Q. Lu, Y. Li and F. Gao, *Chem. Commun.*, 2009, 7542.
18 S. A. Needham, G. X. Wang and H. K. Liu, *J. Power Sources*, 2006, **159**, 254.
19 H. Pang, Q. Lu, Y. Zhang, Y. Li and F. Gao, *Nanoscale*, 2010, **2**, 920.
20 W. Wang, Y. Liu, C. Xu, C. Zheng and G. Wang, *Chem. Phys. Lett.*, 2002, **362**, 119.
21 J.-W. Lang, L.-B. Kong, W.-J. Wu, Y.-C. Luo and L. Kang, *Chem. Commun.*, 2008, 4213.
22 T. Kavitha and H. Yuvaraj, *J. Mater. Chem.*, 2011, **21**, 15686.
23 X. Wang, J. Song, L. Gao, J. Jin, H. Zheng and Z. Zhang, *Nanotechnology*, 2005, **16**, 37.
24 S. Mohan, P. Srivastava, S. N. Maheshwari, S. Sundar and R. Prakash, *Analyst*, 2011, **136**, 2845.
25 A. Ahmadalinezhad and A. Chen, *Biosens. Bioelectron.*, 2011, **26**, 4508.
26 P. R. Solanki, A. Kaushik, A. A. Ansari, A. Tiwari and B. D. Malhotra, *Sens. Actuators, B*, 2009, **137**, 727.
27 S. P. Caudill, G. R. Cooper, S. J. Smith and G. L. Myers, *Clin. Chem.*, 1998, **44**, 1650.
28 P. L. Yeagle, *Biochim. Biophys. Acta, Rev. Biomembr.*, 1985, **822**, 267.

29 J.-C. Vidal, J. Espuelas, E. Garcia-Ruiz and J.-R. Castillo, *Talanta*, 2004, **64**, 655.
30 S. Aravamudhan, A. Kumar, S. Mohapatra and S. Bhansali, *Biosens. Bioelectron.*, 2007, **23**, 2289.
31 J. Singh, P. Kalita, M. K. Singh and B. D. Malhotra, *Appl. Phys. Lett.*, 2011, **98**, 123702.
32 R. E. Dietz, G. I. Parisot and A. E. Meixner, *Phys. Rev. B: Solid State*, 1971, **4**, 2302.
33 P. Chandani, W. Chen and A. Chandani, *Environ. Sci. Technol.*, 2001, **35**, 2562.
34 W. A. Collier and A. L. Hart, *Int. Conf. Sens. Tech.*, 2005, p. 21.
35 S. K. Arya, M. Datta and B. D. Malhotra, *Biosens. Bioelectron.*, 2008, **23**, 1083.
36 H. Dhyani, M. A. Ali, M. K. Pandey, B. D. Malhotra and P. Sen, *J. Mater. Chem.*, 2012, **22**, 4970.
37 S. Srivastava, Md. A. Ali, P. R. Solanki, P. M. Chavhan, M. K. Pandey, A. Mulchandani, A. Srivastava and B. D. Malhotra, *RSC Adv.*, 2013, **3**, 228.
38 A. Wisitsoraat, P. Sritongkham, C. Karuwan, D. Phokharatkul, T. Maturos and A. Tuantranont, *Biosens. Bioelectron.*, 2010, **26**, 1514.
39 N. Ruecha, W. Siangproh and O. Chailapakul, *J. Electron. Sci. Technol.*, 2010, **8**, 82.
40 A. Parra, E. Casero, E. Pariente, L. Vazquez and E. Lorenzo, *Sens. Actuators, B*, 2007, **124**, 30.
41 P. R. Solanki, A. Kaushik, A. A. Ansari and B. D. Malhotra, *Appl. Phys. Lett.*, 2009, **94**, 143901.
42 S. Aravamudhan, N. S. Ramgir and S. Bhansali, *Sens. Actuators, B*, 2007, **127**, 29.
43 Md. A. Ali, S. Srivastava, P. R. Solanki, V. V. Agrawal, R. John and B. D. Malhotra, *Appl. Phys. Lett.*, 2012, **101**, 084105.